CORPUS PUBLISHERS

Journal of Mineral and Material Science (JMMS)

ISSN: 2833-3616

Volume 4 Issue 2, 2023

Article Information

Received date : April 05, 2023

Published date: April 24, 2023

*Corresponding author

Mansurov ZA, Institute of Combustion Problems and Al-Farabi Kazakh National University, Kazakhstan

Key Words

Nanomaterials; Combustion; Graphene; Nanotechnology; Diffusion

DOI: 10.54026/JMMS/1059

Mini Review

Recent Advances and Outlook in Nanotechnology

Mansurov ZA[1,2*] and Nazhipkyzy M[1,2]

[1]*Institute of Combustion Problems, Kazakhstan*

[2]*Al-Farabi Kazakh National University, Kazakhstan*

Abstract

Presented work summarizes recent results of Institute of combustion problems in the field of synthesis of carbon nanomaterials and their application in various areas during the last 5 years: energy intensive nanocarbon materials; electroreduction of AuCl4- in the case of gold electrosorption using activated carbon; bio-waste-derived few-layered graphene/SrTiO3/PAN as an efficient photocatalytic system for water splitting; graphene based membranes for desalination; development and study of perovskite photocatalysts for hydrogen evolution; obtaining of biologically soluble membranes based on polymeric nanofibres and hydroxyapatite of calcium.

Introduction

Nanotechnology refers to the use of nano-scale materials in a range of novel ways. The term "nanotechnology" was introduced by Norio Taniguchi in 1974 during a scientific conference [1]. Metal-Organic Frame Structures (MOFs) are one of the interesting areas in a wide range of applications, including energy-intensive materials. However, a method for producing of these bulk polymers is an expensive and multi-step process. In this regard, it is of interest to search the alternative methods for producing of bulk materials based on multilayered graphenes [2,3]. At the Institute of Combustion Problems has been developed a method for synthesis of multilayer graphene oxide structures (Graphene Oxide Frameworks (GOFs)) from plant wastes such as rice husks or walnut shells. The 21st century will be characterized by a further exacerbation of the shortage of fresh water on the scale of our planet. It is noted that two thirds of drinking water are consumed for the implementation of agro technical measures. At present, a universal trend in therapy and preventive measures against gastric and intestinal diseases is the use of oral (entero) sorbents of different chemical nature which have a high sorption capacity towards binding infectious agents and pathological products of metabolism, thereby exerting an antidote effect. As adsorbing, antidote, and antidiarrheic preparations are widely used in medical practice, creation of their new forms is an important task of medicine. In this regard, the problem of using effective sorbents as a means of delivering medicinal and probiotic preparations is paramount. R. Smalley in his famous article [4] noted 10 urgent problems associated with the development of mankind. Among them are clean air, clean water, energy, health. Fundamental and applied research is carried out in these areas at the Institute of Combustion Problems by our scientists during the last 5 years [4].

The Usage of Graphene Oxide Structures as Energy-Intensive Additives

The resulting activated carbon based on rice husks has a typical surface morphology for samples of plant origin, but has a developed specific surface area (3000 m^2/g) with a large number of micro- and mesopores. Therefore, the structural properties were investigated by various physicochemical methods of analysis. Particular attention should be paid to the Raman spectroscopy method, which makes it possible to evaluate the surface chemistry and topology of the structure of the material under study. Including the number of particles of graphene layers present in the structure, the presence of chemical impurities and structural defects of activated carbon. It is known that Raman spectroscopy is one of the most popular methods for studying carbon nanomaterials such as activated carbon, graphene and nanotubes [5-7]. To study activated carbons, parameters such as a wavelength of 473 nm were used; measurements were made at least 5 points of the sample. As can be seen from the spectra in Figure 1, and the resulting material has typical three peaks (G, D and 2D) for multilayer graphene structures. The calculation of the intensity ratio of the G and 2D peaks allows us to conclude that the graphene film consists of three or more sheets (I2D/IG = 0.63). It should be noted that the width of the peaks is narrow and there are no D3, D4 or D5 peaks, as well as a low noise level indicates the absence of an amorphous structure.

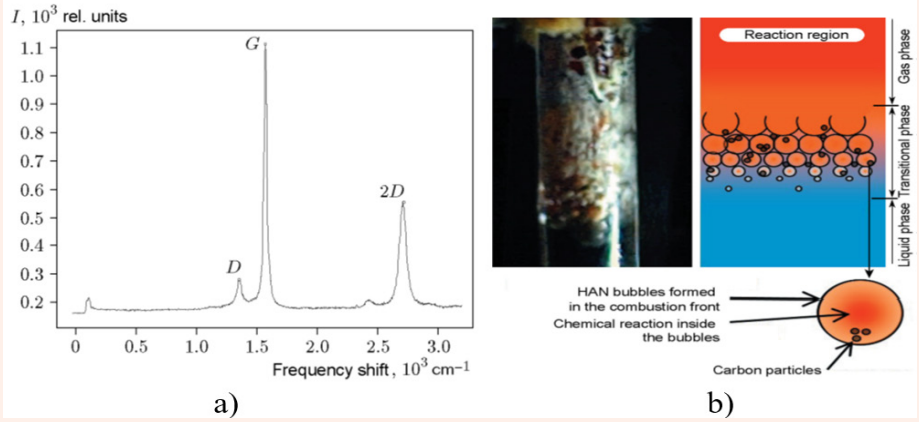

Figure 1: a) Raman spectra of activated carbon obtained from rice husk; b) Propagation of the combustion wave in the case of HAN burning in the liquid phase at p_0 = 6 MPa [8].

Since activated carbon, like other carbon nanomaterials, has a large number of reactive centers, functional groups and heteroatoms on the surface (pores, defects, corners and faces) reinforced with a large specific surface. It can be assumed that it is at these points that heat is accumulated, the electrical conductivity and mass transfer increase, and the decomposition of HAN in the presence of activated carbon, in turn, increases the temperature of the entire system and the reaction propagation rate. Thus, the mentioned parameters undoubtedly play a certain role in increasing the rate of decomposition and, accordingly, the rate of fuel combustion in the presence of activated carbon [8]. Liquid-phase combustion mechanism of HAN with addition of activated carbon at p_0 = 6 MPa is schematically illustrated in Figure 1b. The combustion process of HAN can be characterized as convective combustion, which is characteristic of most single-component liquid fuels. In the presence of activated carbon, the formation of spherical structures during boiling occurs more energetically, due to which a turbulent flame with high speed is formed at the combustion front, which, accordingly, leads to the release of a large volume of combustion products. The combustion process of HAN occurs in three zones: pre-heating, bubble (spherical structures) and gas-gas (reaction zone). It is assumed that the particles of activated carbon located inside the bubbles formed during the boiling of the fuel accumulate a large amount of heat more intensively due to the chemical reaction of the decomposition of the fuel and catalyze the decomposition process of HAN.

Electroreduction Of $AuCl_4^-$ in the Case of Gold Electrosorption Using Activated Carbon

All electrochemical measurements were carried out in a three-electrode cell using an Autolab PGSTAT 302 N galvanostat/potentiostat. A working electrode with surface area of 0.071 cm^2 was represented by the platinum rotating disk Autolab RDE 80725. A platinum plate was used as an auxiliary electrode, and the silver-chloride electrode (Ag/AgCl) was used as a reference electrode. 0.1 mol L^{-1} potassium chloride solution containing $HAuCl_4$ with a pH of 1.5 was served as an electrolyte. The gold chloride solutions with a gold concentration of 7.65; 23.13; 45.34 and 80.79 mg L^{-1} were prepared by dissolution of metallic gold in aqua region. In order to study the kinetics of gold (III) chloride complex adsorption the change in concentration of Au^{3+} was analyzed using the atomic absorption spectroscopy (Perkin Elmer Analyst 200, USA). Cyclic voltammograms were obtained in the study process of gold electroreduction on a platinum electrode from chloride solutions (Figure 2). As can be seen from Figure 2, the cathode peak corresponds to reaction: $AuCl_4^- + 3\bar{e} \rightarrow Au^0 + 4Cl^-$ (1), the anode peak corresponds to the oxidation of gold to Au^{3+}. Complete electroreduction of gold ions proceeds at a potential greater than Ep (c), and electrooxidation at a more positive potential from 800 mV. The dependence of the values of the current density peaks on the square root of the potential scan rate ($\sqrt{\upsilon}$) is linear (Figure 2 Inset) and passes through the origin, which indicates the diffusion nature of the process.

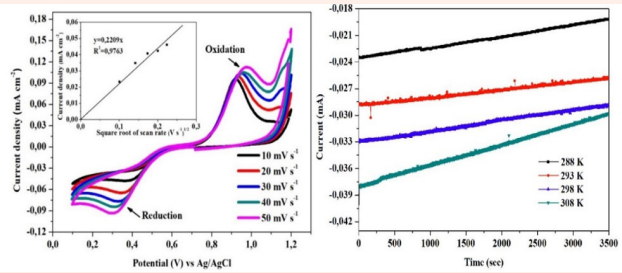

Figure 2: a) Cyclic voltammograms of electroreduction of gold on a platinum electrode in the solution of 80.79 mg L^{-1} $HAuCl_4$ + 0.1 mol L^{-1} KCl at various scan rates, T = 298 K; (b) chronoamperograms of gold electroreduction in the solution of 28.98 mg L^{-1} $HAuCl_4$ (pH = 1.5) at different temperatures with the addition of carbon adsorbent [9].

Activated RH was wrapped with filter paper and then immersed in a thermostatically controlled electrochemical cell with a constant convection. Convection in the cell was provided by a rotating disk electrode. Figure 2a shows that the limiting diffusion currents of the electroreduction of gold ions decrease with time, which indicates a decrease in the concentration of gold ions into the depth of the solution afterwards by its electrosorption by the adsorbent. This trend persists at temperatures from 288 to 308 K. The exception is the chronoamperogram at temperatures of 308 K with a steep slope. It is also clear that the limiting currents at the initial point are directly proportional to temperature, which once again emphasizes the diffusion nature of the process. It is revealed that the electrochemical reduction of gold ions occurring on the surface of the carbon sorbent is limited by diffusion, and this proves the presence of the Randles-Ševčik dependence [10].

Graphene Based Membranes for Desalination

Rice husk, which is a multi-tonnage and renewable waste was used as a raw material to obtain graphene layers. KOH was used as a typical chemical activation agent to induce porosity. The carbon materials containing graphene layers was obtained in four successive stages: pre-carbonization, desilication, activation and exfoliation of the Carbonized Rice Husk (CRH). RH was washed several times with distilled water to remove impurities, and then dried at 383 K for 1 hour. The pre-carbonization of RH was carried out in a rotating reactor in an inert medium (Ar) at a temperature of 523-573 K about 45 minutes, with gas delivery rate of ~ 5 cm^3/min. A series of 5 desilicated samples was mixed with crushed KOH at different temperatures and ratios. The mixtures were compacted in an iron crucible and annealed at 1123 K for 2 h. To protect from oxidation, argon was supplied at a rate of 5 sccm. After activation the resulting samples were washed with distilled water several times to reach the equilibrium of pH~7 and the filtered samples were dried at 373 K for 24 h. The desalination properties of membranes were tested for NaCl, KCl, $MgCl_2$, $CaSO_4$ and $MgSO_4$ using a calibrated Atomic Absorption Flame Emission Spectrophotometer. The initial composition of the salt (35 g/L) solution (sample of seawater) was as follows: NaCl (78.8%), KCl (2.1%), $MgCl_2$ (9.1%), $CaSO_4$ (3.5%) and $MgSO_4$ (6.5%). From Table 1, we can infer that the permeability plays a crucial role on the salt rejection: to a slower process corresponds a better filtration capability. In addition, the poor salt rejection of GF compared to the other two membranes makes it clear that the preparation from graphene oxide (both commercial or from rice husk) by vacuum filtration is much more effective for the production of filtering membranes.

Table 1: Desalination and permeable characteristics of samples.

Membrane	Salts, g/L			Permeability, ml/min (Under Vacuum)	
	Before Filtration	After Filtration	Salt Rejection, %	DI Water	Salt Water (35 g/L)
GOM	35	4	88.5	4	3
GM	35	7	80	5	4
GF	35	32	8.5	30	30

Development and Study of Perovskite Photocatalysts for Hydrogen Evolution

The authors [10] obtained a composite 1D photocatalyst based on $SrTiO_3$/PAN fibers with strong alignment via the electrospinning method. As a photocatalytic material, $SrTiO_3$ with a particle size from 100 to 350 nm was synthesized by compound chemical solution and solid-state reaction [11]. The accepted $SrTiO_3$, with a purity of 97% (Figure 3a), was presented by spheroidal particles with multiple surface pores (Figure 3b). Photocatalysts based on $SrTiO_3$/PAN showed high activity in the splitting of water-methanol under 40W UV radiation with the most elevated yield of hydrogen 305 μmol $h^{-1}g^{-1}$. Further, the activity of these 1D composite photocatalysts based on $SrTiO_3$/PAN was enhanced by the addition of metal oxide particles, which are capable of narrowing the value of their bandgap [11]. Thus, high sintering temperature improves the crystallinity and exposure of the photocatalyst, which leads to the formation of an intermediate hyper-phase, delivering a more efficient split of charge and increasing the efficiency of hydrogen evolution. The consequential photoanode based on $CoTiO_3$ exhibited the yield of hydrogen evolution from 0.5 M KOH solution of 0.3 μmol h^{-1} g^{-1} under the 40W mercury lamp and 0.024 μmol h^{-1} g^{-1} under the xenon lamp.

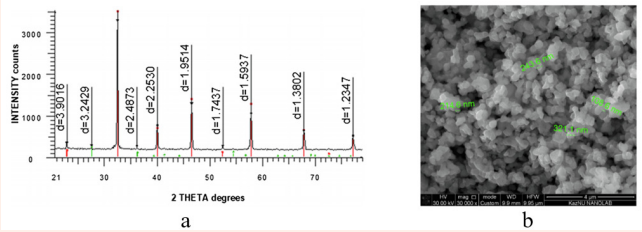

Figure 3: X-ray pattern (a) and SEM (b) of the synthesized $SrTiO_3$ powder. This figure is reprinted from [11], with permission from Elsevier, 2019.

Obtaining of Biologically Soluble Membranes Based on Polymeric Nanofibres and Hydroxyapatite of Calcium

Synthetic HAP was received from biological waste material. The eggshell, including $CaCO_3$, is annealed for 2 to 3 h at a temperature of 900–1000 °C. During annealing, the organic part of the shell burns off, and the resulting precipitate includes CaO as a fine powder without impurities. As a result, crystals with the size of 1–2 microns are created. It is worth noting that studies of the obtained crystalline calcium hydroxyapatite demonstrate that external conditions such as pH, composition, and concentration of reagents and impurities, order and speed of mixing, temperature, and time of the experiment strongly affect the crystallization process and the chemical composition of the synthesized powder. The resulting powdered material is a micron-sized fine powder (1–2 μm).

Structure imperfections due to the presence of vacancies, impurities of implementation and substitution, and determined by them distortions in the crystal lattice became energetically advantageous for the formation of HAP in the hexagonal synonym. Therefore, the existence of micro impurities and other defects in the structure of biological apatite determines its characteristics and affects the physicochemical and chemical-biological properties. Atoms of impurity can be located randomly in the structure of hydroxyapatite. Characterization of the structure of HAP, it is convenient to frame the ideal stoichiometric formula of $Ca_{10}(PO_4)_6(OH)_2$, taking into account the different parts inhabited by calcium atoms in the lattice of HAP as $Ca_{10}(PO_4)_6(OH)_2$, and also calculating the Ca/P ratio, which for our samples was 1.5. The importance of the rate of distribution flow of nutrients relying on the average pore size of the scaffold, which is in the range from 3.92 to 6.26 mm at a certain rotation rate, showed that the geometric shape of the scaffold has a significant effect on the movement of the nutrient fluid. For the G and E scaffolds, the average pore size is 4.12 and 6.26 mm, respectively, but for both scaffolds, the rate of diffusion flow of nutrients is approximately the same - 2.8 ml/h. A careful study of the result of the average pore size of scaffolds on the rate of diffusion flow of nutrients through it at 12 rpm indicates that the pores do not significantly affect the rate of nutrient spread. Such conduct at identical parameters is confirmed in empirical works [12] and perhaps denotes the preference of optimal scaffold rotation rate.

References

1. Taniguchi N (1974) On the basic concept of nanotechnology. Proceedings of the International Conference on Production Engineering, Tokyo, Japan, pp. 18-23.
2. Seo JS, Whang D, Lee H, Jun SI, Oh J, et al. (2000) A homochiral metal–organic porous material for enantioselective separation and catalysis. Nature 404(6781): 982-986.
3. Srinivas G, Burress JW, Ford J, Yildirim T (2011) Porous graphene oxide frameworks: synthesis and gas sorption properties. Journal of Materials Chemistry 21(30): 11323-11329.
4. Smalley RE (2005) Future global energy prosperity: The terawatt challenge. Materials Matters. MRS Bulletin 30: 412-417.
5. Saito R, Hofmann M, Dresselhaus G, Jorio A, Dresselhaus (2011) MS Raman spectroscopy of graphene and carbon nanotubes. Adv Phys 66 (3): 413-550.
6. Atamanov M, Lyu JY, Chen S, Yan QL (2021) Preparation of CNTs coated with polydopamine–Ni complexes and their catalytic effects on the decomposition of CL-20. ACS Omega 6(35): 22866-22875.
7. Atamanov M, Yelemessova Z, Imangazy A, Kamunur K, Lesbayev B, et al. (2019) The catalytic effect of CuO-doped activated carbon on thermal decomposition and combustion of AN/Mg/NC composite. The Journal of Physical Chemistry C 123(37): 22941-22948.
8. Mansurov ZA, Atamanov MK, Elemesova Z, Lesbaev BT, Chikradze MN (2019) New nanocarbon, energy intensive materials. Physics of Comb and Expl 55(4).
9. Supiyeva Z, Avchukir K, Pavlenko V, Yeleuov M, Taurbekov A, et al. (2020) The investigation of electroreduction of $AuCl_4^-$ in the case of gold electrosorption using activated carbon. Materials Today: Proceedings 25: 33-38.
10. Sultanov F, Daulbayev C, Azat S, Kuterbekov K, Bekmyrza K, et al. (2020) Influence of metal oxide particles on bandgap of 1D photocatalysts based on $SrTiO_3$/PAN fibers. Nanomaterials 10(9): 1734.
11. Roy PK, Bera J (2005) Formation of $SrTiO_3$ from Sr-oxalate and TiO_2. Materials Research Bulletin 40(4): 599-604.
12. Daulbayev C, Sultanov F, Aldashev M, Abdybekov A, Bakbolat B, et al. (2021) Nanofibrous biologically soluble scaffolds as an effective drug delivery system. Comptes Rendus Chimie 24(1): 1-9.